PCCP

Accepted Manuscript

ROYAL SOCIETY OF CHEMISTRY

www.rsc.org/pccp

Cite this: DOI: 10.1039/c0xx00000x

www.rsc.org/xxxxxx

ARTICLE TYPE

Bis(μ-oxo) versus mono(μ-oxo)dicopper cores in a zeolite for converting methane to methanol: an in situ XAS and DFT investigation

Evalyn Mae C. Alayon,[a] Maarten Nachtegaal,[b] Andras Bodi,[b] Marco Ranocchiari,[b] and Jeroen A. van Bokhoven*[a,b]

Received (in XXX, XXX) Xth XXXXXXXXX 200X, Accepted Xth XXXXXXXXX 200X
DOI: 10.1039/b000000x

Dicopper species have been identified as the active sites in converting methane to methanol in Cu-zeolites. To understand the formation of these copper cores in mordenite, we used in situ time-resolved X-ray absorption spectroscopy during heat treatment. Significant dehydration enabled the reduction of the copper cores, after which molecular oxygen was cleaved. The activated oxygen bridged two copper atoms to make the reactive precursor for the activation of methane. Even though the active bridging oxygen was detected, the XAS data were unable to distinguish a bis(μ-oxo)dicopper core from a mono(μ-oxo)dicopper core since XAS measures the average structure of the total copper population and the sample contains a mixture of copper species. We therefore used DFT calculations to understand the energetics of the formation of the active copper species and found that if a copper dimer exists in a zeolite, the mono(μ-oxo)dicopper species is an energetically plausible structure. This is in contrast to molecular dicopper cores where the bis(μ-oxo)dicopper core is preferentially formed.

Introduction

Forming methanol selectively from methane at mild conditions is one of the long-standing challenges in chemistry.[1-9] It can be achieved by copper exchanged zeolites,[10,11] although a feasible catalytic process remains to be established. Developing such a process relies on understanding the structure and (re)generation of the copper cores which activate methane.

The formation of the active sites in Cu-MOR initiates the catalytic cycle.[12] These active sites are generated during thermal treatment. Literature suggests that when coordinatively saturated with ligands such as water,[13-15] copper is unable to further coordinate reactant molecules. Therefore, hydrated Cu-zeolites are catalytically inactive at low temperature (< 200 °C). High temperature treatment of Cu-zeolites drives off labile ligands and generates coordinatively unsaturated sites. There are a number of questions in the literature which have yet to be answered unambiguously: how and at what temperature are the active sites formed, which copper sites are involved and to which extent, and which copper species are generated. Disproportionation[16] and condensation[17,18] are the mechanisms proposed to explain the formation of isolated copper ions[19] and dimers[18,20] in a Cu-zeolite, although clusters[21,22] are also created. These different copper species are developed to a different extent depending on the copper loading,[23,24] zeolite topology,[18,25,26] synthesis[27-30] and treatment methods,[25] and display different reactivity and signatures according to the analytical method used,[14,21,31] thereby further complicating a coherent interpretation.

In this article, we focus on Cu-MOR, which has been shown active for converting methane to methanol,[20,32] also in a batch-wise operation under humid conditions.[33] Of particular interest is the identity of the active site and the process of its formation. The active copper cores for methane to methanol conversion on Cu-ZSM-5 were first proposed to be similar in structure to a bis(μ-oxo)dicopper species (Scheme 1a), based on in situ UV-visible measurements by Groothaert and co-workers.[20] Follow-up resonant Raman (rR) measurements on Cu-ZSM-5 combined with DFT calculations led to the modification of the identity of the active site to a bent mono(μ-oxo)dicopper center (Scheme 1b).[24,34] Further investigation into the precursor of these active sites by ^{18}O isotopic labelling combined with UV-visible and Raman spectroscopy suggested that reduced dicopper^{I} pairs, which are formed by high temperature treatment in inert gas, cleave molecular oxygen to form the (μ-η^2:η^2-peroxo)dicopper^{II} precursor. Following electron donation from neighboring Cu^{I} spectator species, the reactive mono(μ-oxo)dicopper core, or [Cu^{II}–O–Cu^{II}] intermediate, is formed.[12]

The dimeric nature of the proposed active copper site in Cu-ZSM-5, and, by extension in Cu-MOR,[20] is strikingly similar to the proposed dicopper active site[35,36] structure in the enzyme particulate methane monooxygenase (pMMO), which efficiently catalyzes the conversion of methane to methanol; hence attention to molecular [Cu^{II}–O–Cu^{II}] complexes is growing.[37,38] pMMO contains a dicopper center in its active site,[35,36] although a distant third copper atom might still be involved for efficient O-atom transfer.[39-41] Optical spectroscopic studies on the interaction of oxygen with the active dicopper site in pMMO revealed that the active complex takes the form of the (μ-η^2:η^2-peroxo)dicopper core.[42]

Dicopper cores are also found in molecular complexes and some of them are well characterized by single crystal X-ray

crystallography.[43,44] Dioxygen activation at Cu^I mononuclear centers can form (μ-η^2:η^2-peroxo)dicopper[45,46] or bis(μ-oxo)dicopper[47-49] structures depending mostly on the ancillary ligands. Sterically demanding tripodal ligands such as substituted hydrotris(pyrazolyl)borates favor peroxodicopper complexes, whereas strong σ-donor bidentate ligands such as tetraalkyldiaminocyclohexanes favor bis(μ-oxo)dicopper sites. It is accepted that bis(μ-oxo)dicopper activate intra- and intermolecular aromatic C–H bonds and that peroxodicopper complexes do this intramolecularly only under favorable electronic and steric conditions.[50,51] On the other hand, mono(μ-oxo)dicopper complexes are less common and are obtained by cooperative 4-electron reduction of the dioxygen molecule with four Cu^I ions,[52] or from 2 equivalents of Cu^I compound and an equivalent of an oxygen transfer agent.[53-56] The likelihood of forming the mono(μ-oxo)dicopper core is low because of the strong electron density that the oxido ligand experiences from the electron-rich Cu^{II} centers, making it particulary reactive, for example to water, that turns it into a bis(μ-hydroxo)dicopper core.[57]

While molecular mono(μ-oxo)dicopper cores are rare and poorly characterized, they are established intermediates for methane to methanol conversion in Cu-zeolite as described above. For Cu-zeolites, the (μ-η^2:η^2-peroxo)dicopper core is both the proposed "inactive" isomer of the bis(μ-oxo)dicopper core[20] and precursor to the active mono(μ-oxo)dicopper site.[12,58] It follows that if a dicopper site is formed in Cu-MOR, active for methane to methanol conversion, it is compelling to discern between bis(μ-oxo)dicopper and mono(μ-oxo)dicopper cores during its formation.

We previously reported X-ray absorption spectroscopy (XAS) data taken of Cu-MOR during methane activation[59] and proposed that about half of the total copper atoms changed structure. This was in agreement with the recent results of Vanelderen and co-workers, who used complementary temperature programmed reduction, H_2 pulse chemisorption, UV-Vis/NIR and EPR spectroscopies, showing that about 60% of the total copper content make up the binuclear autoreducible fraction.[60] We also showed how these copper species changed structure during desorption of the methane conversion intermediate as methanol in the presence of water.[33] Here, we will show how the reactive copper cores are generated during treatments prior to methane activation by following the real time changes to the copper structure through time resolved XAS measurements, thus allowing insights into the mechanisms of dehydration, autoreduction and activation of molecular oxygen. Further, we use complementary density functional theory (DFT) calculations to identify energetically plausible structures of the active copper site, both for molecular complexes and Cu-zeolite systems.

Experimental Details

I. Sample preparation and XAS measurements

Cu-MOR was synthesized by aqueous ion exchange from copper acetate and Na-mordenite. The synthesis and characterization steps were described in detail in a previous publication.[32] XAS measurements were performed at the SuperXAS beamline, Swiss Light Source of the Paul Scherrer Institute in Villigen, Switzerland. Around 15 mg (250–500 μm sieve fraction) of Cu-MOR was sandwiched between two quartz wools and placed in a 3 mm diameter, thin-walled (0.1 mm) quartz capillary reactor. This was attached to an air blower set-up for controlled heating. Gas flows were controlled by mass flow controllers . All gas lines were heated to 110 °C to prevent condensation. Gases of grade 4.5 to 5.0 were used. Thermal treatment in oxygen involved heating Cu-MOR at 1 °C/min from room temperature until 450 °C in 30 mL/min of flowing oxygen. Thermal treatment in helium (quality 5.0, contains 1 ppmv O_2 and 3 ppmv H_2O) consisted of heating Cu-MOR at 5 °C/min in 30 mL/min of flowing helium from room temperature to 450 °C. Reduction of Cu-MOR employed a 30 mL/min flow of 5% H_2/He while heating at 5 °C/min. A quadrupole mass spectrometer (MS) was attached to the exhaust line of the capillary reactor to monitor the composition of the gas stream leaving the catalyst bed.

The X-ray beam, sample, and X-ray detectors were in conventional transmission geometry. A quick scanning channel-cut Si(111) monochromator selected the energy of the incoming beam.[61] An XAS spectrum was collected every 10 seconds. Spectra of copper foil were collected simultaneously for internal energy calibration

II. XAS data analysis

After assigning the spectra to the corresponding reaction conditions and MS data, standard data reduction steps[62] were performed using the data analysis software XDAP.[63] These involved background subtraction, normalization, calculation of the EXAFS (χ) function, and Fourier transformation of the EXAFS to generate a pseudo radial distribution function, hereon referred to as FT EXAFS. Five quick XAS spectra were averaged to improve the signal to noise ratio of a spectrum for EXAFS fitting. Theoretical Cu–Cu and Cu–O references were generated from crystallographic structures of bulk copper and $copper^I$ oxide, respectively. The theoretical phase and backscattering amplitudes for Cu–Cu and Cu–O absorber-backscattering pairs were generated using the FEFF8 code.[64] In the XDAP program fitting routine, the Debye-Waller factor DW and edge-shift ΔE_0, are given as an offset with respect to the reference.[62] The theoretical references were optimised so that the offsets of DW and ΔE_0 to those of measured copper foil and $copper^I$ oxide spectra were approximately zero. The value of the amplitude reduction factor S_0^2 was determined by fitting the theoretical Cu–Cu and Cu–O spectra to the first coordination shells of the measured spectra of copper foil (1.0 Å < R < 3.0 Å, 2.7 $Å^{-1}$ < k < 10.5 $Å^{-1}$, k^2, $S_0^2 = 0.77$) and $copper^I$ oxide (0.7 Å < R < 2.2 Å, 2.7 $Å^{-1}$< k < 10.5 $Å^{-1}$, k^3, $S_0^2 = 0.60$). Fitting the optimised theoretical Cu–Cu and Cu–O scattering pairs to the measured EXAFS functions in XDAP (0 Å < R < 4.5 Å, 3.2 $Å^{-1}$ < k < 10.4 $Å^{-1}$, k^2) generated fitted values for coordination number N, Debye-Waller factor DW, interatomic distance R, and edge-shift ΔE_0.

A linear combination fit (LCF) procedure was performed on the normalized XANES spectra (–20 to 50 eV) using the IFEFFIT software package.[65] The reference spectra used for the LCF were XANES spectra of Cu-MOR after ion exchange, after calcination at 450 °C, after hydrogen treatment at 200 °C, and after hydrogen treatment at 450 °C, to represent the copper species in Cu-MOR in the hydrated Cu^{II}, fully dehydrated and oxidized Cu^{II}, reduced Cu^I, and fully reduced Cu^0 states, respectively (see Figure S1-1).

III. Calculations

The energetics of the active [Cu^{II}–O_2–Cu^{II}] and [Cu^{II}–O–Cu^{II}] sites was studied by DFT using Gaussian09.[66] When coordinated to bulky organic ligands, copper readily forms isolated bis(μ-oxo) complexes. This is in contrast with the proposed mono(μ-oxo) active site configuration in zeolites. Calculations were carried out on Cu_2O_2 and Cu_2O structures of the Large Lattice Model (LLM) of Woertink et al.,[34] shown in the mono(μ-oxo) state as [**1**-LLM]–O in Scheme 2 with the terminal OH groups marked as dashed bonds. Two molecular dicopper complexes were also studied: structure **5** by Mahadevan et al. is a doubly charged copper(III) complex,[67] shown in the bis(μ-oxo) state as [**2**]–O_2 in Scheme 2. Furthermore, calculations were carried out on structure **2** by Straub et al.,[68] denoted in the bis(μ-oxo) state as [**3**]–O_2 in Scheme 2, a neutral copper(III) complex. In [**1**-LLM] geometry optimizations, the eight Si atoms were constrained at their crystallographic positions in ZSM-5 by Olson et al.[69] In the geometry optimizations of the isolated complexes [**2**] and [**3**], the four N atoms were first constrained, and then freed in a subsequent optimization to study geometry relaxation effects. Several exchange–correlation functionals were used, including the widely used B3LYP functional,[70] B97D containing dispersion corrections,[71] the M06-2X functional of Zhao and Truhlar,[72] and the PBEh1PBE functional.[73] In addition to Pople's 6-311+G(d) and Ahlrich's def2-SVP and def2-TZVP basis sets,[74] we also used the LANL2DZ and LANL2TZ(f) basis sets with effective core potentials on copper.[75] Zero-point energies were calculated using B3LYP/def2-SVP on H, C, N, O, P and Si, and LANL2DZ on Cu for [**2**] and [**3**], and B3LYP/6-311+G(d) in LLM calculations. Solvent effects on the relative stability of bis(μ-oxo) vs. mono(μ-oxo) complexes were studied in ethanol using the PCM model on neutral [**2**] and [**3**].[76]

Results and Discussion

I. Description of starting Cu-MOR material

Synthesis by aqueous ion exchange of copper acetate and Na-mordenite was intended to exchange hydrated copper ions in solution with the sodium ions in the zeolite to provide well-dispersed copper species in ion-exchange sites of mordenite. Our attempt to determine the copper dispersion by transmission electron microscopy (TEM), however, gave ambiguous information regarding particle size of the copper species since the collected TEM images showed different dispersions from one to the other (see Figure S2).[11] An X-ray diffractrogram of Cu-MOR, which was published before,[32] showed reflections that belong only to the crystalline mordenite structure, hence, crystalline copper and copper oxide particles larger than about 3 nm can be excluded.

Figure S2-2 shows the XAS spectra taken of Cu-MOR after synthesis. It shows the characteristics of hydrated Cu^{II} species. Kau and co-workers reported an extensive study of the effect of ligand coordination on the shape of the Cu K-edge XANES spectra that serves as the basis for the following peak assignment.[77] The presence of a weak pre-edge feature at 8977 eV and the localization of the main rising edge feature around 8987 eV are indicative of Cu^{II}. The high intensity at 8997 eV is characteristic of octahedral Cu coordination. The features at the XANES rising edge (8979–8987 eV) are influenced by both copper oxidation state and copper coordination environment.[18,25,29,78,79] They manifest the $1s \rightarrow 4p$ transition combined with simultaneous shakedown transitions from a high energy ligand orbital to the Cu $3d$ core hole.[80]

The Fourier transformed EXAFS spectrum of Cu-MOR at room temperature, either in helium or oxygen, showed an intense coordination shell centered around 1.5 Å (not corrected for phase shift) and almost featureless higher shell structure (Figures 3 and S3-2c). The fit of these spectra showed three to four oxygen backscatterers at 1.94 Å (Tables S4-1, and S4-2) with no other contributions in the fitted range. These results are similar to earlier findings of Kuroda and co-workers of Cu-MOR at 300 K.[22] The absence of strong contributions in the higher coordination shells suggested either that different backscattering contributions are cancelling each other out, or more probably, that no heavy neighbors were present and implied fine dispersion of copper species in the MOR framework. The copper species in Cu-MOR after synthesis by aqueous ion exchange and drying at 110 °C are known to be composed mostly of hydrated Cu^{II} sites,[16] with copper coordinating to oxygen, water and OH ligands. Electron paramagnetic resonance studies in the literature further showed that these copper species are mobile.[16]

II. Motivation for thermal treatments in oxidative and inert atmospheres

Calcination of Cu-MOR at 450 °C eliminates residual organic matter and activates the copper sites for methane to methanol conversion. The loss of coordinating water or OH ligands and formation of new bonds with oxygen leads to the formation of the active oxygenated copper sites. Disproportionation and condensation are proposed to precede the formation of catalytically active copper sites. Scheme 3 shows the corresponding disproportionation and condensation reaction mechanisms. Disproportionation assumes that the release of a hydroxyl radical is involved, leading to the formation of isolated copper sites.[16] A [Cu^{II}OH] species reduces to [Cu^{I}] with the release of a hydroxyl radical and reacts with another [Cu^{II}OH] to generate [Cu^{II}O] and water. In condensation, two neighboring [Cu^{II}OH] species condense to eliminate water and form [Cu^{II}–O–Cu^{II}]. This is followed by the reduction of both Cu^{II} ions to a dicopper species with an oxygen vacany [Cu^{I}–Ø–Cu^{I}]. Water release and copper reduction are involved in both condensation and disproportionation mechanisms. Investigation into the mechanism of oxygen activation to form the reactive intermediate by Smeets and co-workers using UV-visible and resonant Raman spectroscopy suggested that the reaction of oxygen with thermally treated Cu-ZSM5 forms the (μ-η^2:η^2-peroxo)dicopper^{II} precursor, which readily transforms into the mono(μ-oxo)dicopper^{II} core with the aid of two electrons from spectator Cu^{I} species.[12] These findings are summarized in Scheme 4, which shows a probable pathway for the synthesis of active sites by thermal treatment. The dehydration of copper sites by thermal treatment drives autoreduction. The resulting reduced and undercoordinated copper sites cleave molecular oxygen to form the oxygenated active copper sites.

Thermal treatment in oxygen is a pre-requisite for methane activation, but it also prevents the observation of the phenomenon

by which the copper sites activate molecular oxygen by XAS since the Cu^{II} state is preserved. Monitoring the XANES features during heating in helium allowed us to observe autoreduction, which follows from the removal of hydroxyl and water ligands, and redox changes during the activation of molecular oxygen and the activation of methane. Comparing the XANES features during heating in helium with those of heating in oxygen allowed us to determine the temperature for autoreduction, which is the minimum temperature required for active site formation.

a) XANES during thermal treatments

Figure 1 compares the XANES spectra taken of Cu-MOR during progressive heating in oxygen (Figure 1a) to those taken during heating in helium (Figure 1b). For each treatment, a new sample was used. The XANES recorded during heating in oxygen showed a progressive decrease in the maximum absorption feature around 9000 eV, which is an indication of the gradual change in the first coordination shell of copper with temperature. The localization of a distinct shoulder around 8986–8987 eV and the pre-edge feature at 8978 eV were attributed to a constant Cu^{II} oxidation state. This calcination caused the copper sites to lose their labile water and OH ligands, which was reflected as loss of oxygen coordination by dehydration. The loss in whiteline intensity is similar to the behaviour of $Cu(NO_3)_2$ when the water ligands are removed.[81] The splitting[82] and shift of the rising edge to lower energy indicate a structural change of the copper species from distorted octahedral, $Cu(OH)_2$-like[83] to distorted planar, CuO-like,[84] minus the long-range order of crystalline CuO (*vide infra*). Reports in the literature show that a fraction of these calcined copper species takes the form of $[Cu^{II}–O–Cu^{II}]$ clusters, active for methane to methanol conversion.[12,58,60]

The spectra taken during heating in helium also showed a progressive decrease in the 9000 eV feature and development of the 8987 eV rising edge and 8978 eV pre-edge features. There was an additional development of a rising edge feature at 8983 eV, assigned to a Cu^{I} contribution, whose tail contributed to the background intensity of the 8978 eV pre-edge feature. The overall shape of the spectrum after thermal treatment in helium is indicative of dehydrated copper in a mixed Cu^{I}/Cu^{II} state.

b) Linear combination fitting of the XANES spectra

Figure 2 shows selected features from the XANES spectra taken of Cu-MOR during heating in oxygen (black squares) and helium (red circles). The edge position (E_0, Fig. 2a), taken as the energy at the maximum of the first derivative of the XANES spectrum, is an indirect indicator of the formation of a distinct shoulder at 8986 eV, characteristic of Cu^{II}. The more pronounced the 8986 eV shoulder, the more the edge position shifts to lower energy. For Cu-MOR in oxygen, the edge was centered at 8986.4 eV at room temperature. Starting around 80 °C, the edge shifted by around 1 eV, and stayed at 8985 eV until the end of the heating ramp at 450 °C. Meanwhile, the intensity of the maximum absorption feature at 8996 eV (Fig. 2b) decreased steeply from room temperature to 200 °C, and decreased more gradually afterwards. The heating period up to 200 °C corresponded to a major loss of bulk water and water in the hydration sphere of copper.[21] The rate of change in the intensity of the maximum absorption feature decreased after 250 °C, implying that rather small changes were taking place in the local geometric coordination sphere of copper. For Cu-MOR in helium, the edge position underwent a continuous decrease in energy until 150 °C, after which it remained at the same position until around 300 °C. The edge position during treatment in helium shifted to lower energy by around 1.5 eV at 305 °C, contrary to the treatment in oxygen, during which it remained almost constant at 8985 eV. The decrease in the intensity at the maximum absorption feature was similar to that of treatment in oxygen: rapidly decreasing until 200 °C and decreasing slowly thereafter. The intensity of the 8983 eV Cu^{I} feature started to increase at 120 °C and continued to do so until 450 °C. The intensity contribution of the 8983 eV feature to the rising edge became significant at high temperatures, causing the edge position to shift at 305 °C. This implied that a significant reduction of the copper sites took place already at 305 °C.

The reduction of copper ions precedes the formation of copper dimers by thermal treatment, either in vacuum or in inert gas.[25] Therefore, following the extent of reduction translates to following the extent of active site generation. Semi-quantification of the amount of reduced copper that contributes to the XANES spectra may be carried out by the use of a linear combination fitting (LCF) procedure. Figure 2d shows the LCF results for the XANES spectra taken during heating in oxygen and those taken during heating in helium. For both treatments, the hydrated Cu^{II} component (filled symbols) decreased steeply from room temperature (100%) until 200 °C (20% in O_2, 8% in He). Simultaneously, the dehydrated Cu^{II} component (empty symbol) increased steeply until 200 °C to comprise 80% of the copper sites (80% in O_2, 77% in He). Some additional reduced Cu^{I} component (crossed symbol, 11–16%) was found for Cu-MOR treated in helium at temperatures up to 200 °C. The significant difference in structure of Cu-MOR between O_2 and He treatments was seen during thermal treatment above 200 °C. The thermal treatment in oxygen brought about the formation of more oxygenated (and dehydrated) Cu^{II} sites, which was the remaining 20% of the composition of the calcined state. Thermal treatment in helium increased the amount of the Cu^{I} component from 15% at 200 °C to 43% at 450 °C, while it decreased the Cu^{II} component from 77% at 200 °C to 57% at 450 °C.

c) EXAFS spectroscopy during thermal treatments

Figure 3 shows the Fourier transformed (FT) EXAFS spectra taken during heating in oxygen and helium, with both real and imaginary parts displayed. The fit results, in terms of the development of the coordination number and interatomic distance, are presented in graphical form in Figure 4. The numerical values of the fit parameters are shown in the supporting information (Tables S4-1 and S4-2). The fits for the spectra series during heating in oxygen identified four coordination shells: a first coordination shell of oxygen, a second coordination shell of another oxygen, a third coordination shell for copper, and a fourth coordination shell for another copper scattering contribution, designated in Figure 4a-b as 1-O_1, 2-O_2, 3-Cu_1, and 4-Cu_2, respectively. The FT EXAFS spectra of the starting materials (Figure 3), both in oxygen and helium, were characterized by a pronounced peak around 1.5 Å (uncorrected for phase shift), which was attributed to the nearest oxygen neighbors. Heating in oxygen from room temperature until 450 °C was accompanied by a decrease in the intensity of the first

coordination shell of oxygen atoms (1-O_1, Figure 4) due to the loss of coordinated oxygen ligands. Physisorbed water and water complexed to transition metal sites are reported in the literature to be removed between 40 °C and 174 °C.[85] The imaginary part of the spectra at the first coordination shell was similar in shape throughout the data series, which suggests that the same oxygen backscatterer remained. Differences were observed at the features between 2 to 3 Å ($R + \Delta R$), where a 2nd coordination shell developed after heating to 75 °C. This feature was fitted with a single copper scatterer (3-Cu_1, N = 0.9) at 2.90 Å, and stayed almost constant until 450 °C (N = 1.2, R = 2.92 Å). The loss of water ligands by heating causes the copper atoms to interact with the framework oxygen atoms of the zeolite and/or to form copper dimers. Starting at 200 °C, a broad feature between 3.5 to 4.0 Å ($R + \Delta R$) became perceptible and this was fitted with two copper scatterers (4-Cu_2, N = 2.0) at 4.36 Å, consistently until 450 °C (N = 2.0, R = 4.40 Å). At 300 °C, the 2nd coordination shell started to show assymmetry, which became more prominent with increasing temperature. The spectrum at 300 °C was fitted with an additional fractional oxygen contribution (2-O_2, N = 0.2, R = 2.42 Å) in between the 1st oxygen and copper neighbors. This oxygen appeared upon reaction of gaseous molecular oxygen, which reacted with undercoordinated copper sites generated at high temperature. In ZSM-5, loss of bulk water was reported to be complete at 250 °C and that OH condensation occurs between 300 °C to 350 °C.[21] The FT EXAFS of the calcined Cu-MOR at 450 °C showed a geometric structure that is similar to the one at 300 °C in which the copper atoms are coordinated to oxygen atoms of the zeolite framework (1.90 Å, 1-O_1), a fraction of a longer oxygen (2.37 Å, 2-O_2), a single copper neighbor for the dimer (2.92 Å, 3-Cu_1), and a couple of extended copper neighbors (4.40 Å, 4-Cu_2). The fits for the spectra series during heating in helium, on the other hand, identified only three coordination shells: a first coordination shell of oxygen, a second coordination shell of copper, and a third coordination shell for another copper contribution, designated in Figure 4c-d as 1-O_1, 2-Cu_1, and 3-Cu_2, respectively. The observations that only a fractional amount of oxygen was found at 2.37 Å and the presence of distant copper neighbors suggest that multiple types of copper species exist, such as ions, dimers, and clusters.

Heating in helium also showed intensity loss at the first coordination shell, with the imaginary part of the FT unchanged. Similar to heating in oxygen, this was linked to the loss of nearest neighbor oxygen atoms (1-O_1) by dehydration. The low intensity feature(s) around 2.6 Å ($R + \Delta R$) gave rise to a distinct peak (2-Cu_2) after heating at 75 °C, which was fitted to a fraction of one copper neighbor (N = 0.5) at 2.95 Å. The shape of this feature at 300 °C did not reflect the assymmetry observed for that in an oxygen atmosphere, and was fitted to a copper contribution until high temperature. A weak 3rd coordination shell was fitted with a more distant copper scatterer (3-Cu_2, N = 3.7, R = 4.4 Å). The similar localization of the nearest neighbor oxygens at 1.94 Å ($R + \Delta R$), whether in oxygen or helium, suggested that these belong to the anchoring zeolite framework oxygen atoms. The presence of the bridging oxygen scatterer at 2.4 Å during heating in oxygen, and its absence when the atmosphere is helium suggests that this bridging oxygen is picked up by the copper sites from the feed stream after sufficient activation. This agrees to the XANES data (Figure 2a) where sufficient autoreduction was observed at 305 °C under a stream of helium to cause the edge energy to decrease by 1.5 eV, and to the EXAFS (Table S3-1) where the bridging oxygen was fitted starting at 300 °C, which means that it is formed in a sufficient quantity to be visible in the spectra at this temperature. The presence of the distant copper scatterers at 4.4 Å, whether in oxygen or helium thermal treatments, agrees to the earlier notion of the inherent existence of multiple copper species in the zeolite.

III. Calculated energetics: mono(μ-oxo) vs. bis(μ-oxo) and peroxo dicopper species

The collected XAS data showed that activation of copper sites for methane to methanol conversion is accompanied by significant dehydration, followed by activation of molecular oxygen. The activated oxygen bridges copper dimers. The EXAFS fits described the copper cores as anchored to about three oxygens of the zeolite, coordinated to approximately a single copper neighbor, and a bridging oxygen. This indicates that the dicopper structure represents the majority of the copper species present in activated Cu-MOR.[59,60] The XAS data are, however, insufficient by themselves to distinguish a bis(μ-oxo)dicopper structure from that of a mono(μ-oxo)dicopper species conclusively, since they measure an average structure for the total copper population. Isolated copper ions and clusters might also contribute to the average structure.

The active site in Cu-zeolite has previously been proposed to be a mono(μ-oxo)dicopper core through resonant Raman measurements and complementary DFT calculations.[34] However, analogous complexes in the homogeneous phase are typically bis(μ-oxo)dicopper structures. On the one hand, there are obvious mechanistic reasons for this discrepancy. In the homogeneous phase, once an oxygen molecule coordinates to copper, there is no apparent exit path for a single O atom to allow for the formation of a mono(μ-oxo) dicopper product. In the zeolite, on the other hand, it is easily possible that the O–O bond will be cleaved after the oxygen molecule has coordinated to the copper site, particularly so if there is an exoenergetic path to coordinate the second oxygen atom nearby.

Density functional calculations unveil the energetics of the mono- and bis(μ-oxo) sites and are summarized in Table 1 with the sites being shown in Figure 5. The full structures for all species are shown in Figure S4-1. For the homogeneous complexes, the energetics of the [**2**/**3**]–O + ½O_2 → [**2**/**3**]–O_2 are reported. The electronic ground state was found to be singlet with the exception of the neutral bis(μ-oxo)dicopper(II) complex [**2**]–O_2 and the oxygen molecule, which are both triplets. Fully optimizing the complex geometries, including solvent effects and considering zero-point effects influence the predicted 0 K reaction energy, but not by as much as the choice of basis set and exchange–correlation functional. However, all calculations predict the bis(μ-oxo) core to be more stable in the homogeneous phase, and therefore there is no thermochemical driving force to make mono(μ-oxo) cores in these molecular complexes.

The picture changes when the zeolite sites are considered in [**1**-LLM] with triplet electronic ground states throughout. From the μ-(η^1:η^2)-peroxo-dicopper and trans-μ-1,2-peroxo-dicopper [**1**-LLM]–O_2 structures shown in Figure 5(e,f), the (e) minimum is analogous to the two third-nearest-neighbor structure found by

Yumura et al., obtained using periodic boundary condition DFT calculations with the B3LYP functional (see Figure 3 in Yumura et al.)[86] Our B3LYP calculations suggest that the (e) minimum is almost isoenergetic with (f) at an energy difference of 12 kJ mol^{-1}, and but the M06-2X functional predicts an energy difference of 61 kJ mol^{-1}, with (e) being more stable. We have been unable to locate the third nearest neighbor bis(μ-oxo) minimum in LLM, which may be due to the inflexibility of the lattice, in which the silicon atoms are frozen at their crystallographic positions. However, the resulting O_2 binding energy in LLM of about 230 kJ mol^{-1} is commensurate with the binding energy in the third-nearest neighbor bis(μ-oxo) species of 220 kJ mol^{-1} as reported by Yumura et al. Based on these results, even the analogous process to the one in homogeneous complexes, in which the mono(μ-oxo) core is oxidized, turns out to be mildly endothermic (Table 1). On the zeolite surface, a self-evident reaction route is the disproportionation of two [**1**-LLM]–O sites to form [**1**-LLM]–O_2 and [**1**-LLM]–Ø. This reaction is substantially endothermic (Table 1), which means that there is a strong pull effect for the inverse process, i.e. the formation of mono(μ-oxo) core from O_2-sites in the presence of free copper sites is strongly favored. The high exothermicity of this reaction means that two mechanisms can be considered as to how the second oxygen atom reaches the free copper dimer site. Either the zeolite pore mediates oxygen atom transfer or the peroxodicopper species can form ozone, which then readily oxidizes the free copper site to yield the second mono(μ-oxo) site.

IV. Summary and comparison with literature

The changes in the composition of the Cu sites during thermal treatment suggest that significant dehydration (~80%) takes place until 200 °C regardless of gas environment. Above 200 °C, the remaining fraction of the hydrated [Cu^{II}] sites reduce to [Cu^{I}] in the absence of oxygen while eliminating a small amount of water. In the presence of oxygen, the remaining hydrated [Cu^{II}] sites dehydrate and contribute to the oxygenated (dehydrated) fraction. In the literature, the reduction of [Cu^{II}–OH] sites to [Cu^{I}–Cu^{I}] pairs has been accepted as necessary to provide for the possibility to activate molecular oxygen.[12] During heating in oxygen, the simultaneous (dehydration and) reduction of copper sites and activation of molecular oxygen take place to provide the active copper sites. The minimum activation temperature in oxygen was previously determined to be 350 °C from the formation of the 22700 cm^{-1} band, which was attributed to the active site [Cu–O–Cu] in Cu-ZSM-5.[24] In our data set, 350 °C corresponds to the condition where already 96% of the Cu sites in oxygen are in the dehydrated Cu^{II} state. At this same temperature, 33% of the copper sites are reduced in helium. That Cu-MOR exhibited a different UV-Vis band (at 22000 cm^{-1}) for the active site, and yielded a larger amount of methanol compared to the proportion of the UV-Vis band intensity was suggestive of the possibility of an additional or different active site.[24] LoJacono and co-workers, who used magnetic susceptibility and optical diffuse reflectance spectroscopy to complement EPR measurements on Cu-ZSM-5, proposed that the EPR-silent bridge [Cu^{II}–O–Cu^{II}] species, may only amount to 20 % of the total Cu composition.[21] The data presented here showed that at 450 °C about 43 % of Cu^{I} forms, which is the fraction that can possibly form the [Cu^{II}–O–Cu^{II}] sites. Palomino and co-workers,[18] who used XAS showed that dehydration until 200 °C causes rearrangement of cupric species in the channels of zeolite ZSM-5 while oxygen elimination beyond 200 °C causes reduction of the cupric ions. The data presented here are in agreement with significant dehydration until 200 °C and significant reduction thereafter. However, in contrast to their results showing no reduction below 200 °C, dehydration of our Cu-MOR material below 200 °C was already accompanied by a small degree of reduction. Llabres i Xamena showed that reduction of Cu-MOR by heating in vacuum until 400 °C was not complete. Their estimate from the XANES data showed that 30 % of the Cu sites were in the Cu^{II} state after heating in vacuum until 400 °C.[25] These account for the EPR silent [Cu^{II}–O–Cu^{II}], which are underestimated with EPR data compared with the estimate from XANES spectra. Around 57 % of the copper species in the Cu-MOR used in this study were in the Cu^{II} state after heat treatment in inert gas at 450 °C, approximately double compared to the reported 30 % value. This difference may have originated from different synthesis methods or manner of reduction. Palomino and co-workers employed the intensity at the maximum of the first derivative of the Cu^{I} XANES spectrum of Cu^{I}-ZSM5 derived from gas-phase exchange of CuCl to quantify the fraction of Cu^{I} species in the Cu-MOR sample. They also used heat treatment in vacuum while the method used in this study was thermal treatment in helium.

Our experiments performed on Cu-MOR on the dependence of the activation temperature with the formation of MeOH, where tests where carried out in the 200–450 °C temperature range showed that a minimum activation temperature of 350 °C was required to observe MeOH in the gas phase. This method is, however, also dependent on the sensitivity of the system to detect MeOH. For the small quantities involved, a big error margin should be considered. Thus, the formation of a fraction of the active sites for methane to methanol conversion, which comprise around 28 % of the total copper sites, occur over a temperature range starting immediately after dehydration of the copper sites above 200 °C (Figure 2d). 10–16% of the total copper sites, which are active, are already formed below 200 °C. The observation that a similar structure was achieved by heat treatment in hydrogen until 200 °C is a second line of evidence for the existence of this minimum temperature. The total amount of reducible copper, which is 43%, constitute the species capable of activating molecular oxygen and catalyze the activation of methane. Indeed, we have shown in previous contributions[59] that a large fraction of copper sites (> 40 %) reduce upon interaction with methane.

Comparing the energetics of oxygenated dicopper sites in homogeneous complexes and on the zeolite, there is no thermochemical driving force toward mono(μ-oxo) structures in the molecular copper complexes. In the presence of nearby free copper sites, they are formed in highly exothermic reactions on the zeolite. We speculate that the steric hindrance and constraints of the MOR framework contribute to the relative stabilization of the mono(μ-oxo)dicopper species and makes bis(μ-oxo) formation unfavorable.

Conclusions

Dicopper cores in copper-zeolites are proposed to constitute the

active sites for methane to methanol conversion. The aim of this paper was to understand the formation of these active dicopper core in Cu-MOR. XAS analysis showed that thermal treatment of Cu-MOR induces dehydration of the copper sites that is mostly completed at 200 °C. If the thermal treatment is done under oxygen up to 450°C, the active copper species, where activated oxygen bridges a copper dimer, is formed. Heating in helium allowed observation on the conversion of copper sites into Cu^{I} species above 200 °C through dehydration and autoreduction. The reducible species account for around 43% of the total copper sites that may cleave molecular oxygen and form the binuclear active site for methane activation.

Even though the bridging oxygen is detected in the Fourier transform, the data from XAS are, however, insufficient to distinguish between the bis(μ-oxo) and the mono(μ-oxo)dicopper structures as the exclusive species in Cu-MOR because XAS measures the average structure of the total copper population, which may be a mixture of different copper species. DFT energy calculations confirmed that the bis(μ-oxo)dicopper structure is favored in homogeneous complexes. On the other hand, the mono(μ-oxo)dicopper structure is strongly favored at the copper dimer site in the zeolite. This shows that the coordination environment in a zeolite is distinct from that of a molecular complex, implying that future work for the development of a catalytic process should be driven by the particular behavior of the active sites on solid supports.

Acknowledgements

We thank Dr. Frank Krumeich for the TEM measurements, Javier Alonso-Mora for developing a Matlab code for QuickXAS data series normalization. Thanks are also extended to beamtime support by Christian Koenig, Min Wei Tew, Zhiqiang Ma, and Jagdeep Singh.

Notes and references

[a] *ETH Zurich,Vladimir-Prelog-Weg 1, Zurich, CH-8093 Switzerland. Tel: 41 44 632 5542; E-mail: jeroen.vanbokhoven@chem.ethz.ch*
[b] *Paul Scherrer Institute, Villigen, CH-5232 Switzerland. Tel: 41 56 310 5046; jeroen.vanbokhoven@psi.ch*
† Electronic Supplementary Information (ESI) available: See DOI: 10.1039/b000000x/

1. A. E. Shilov and G. B. Shul'pin, *Chem. Rev.*, 1997, 97, 2879-2932.
2. R. A. Periana, D. J. Taube, S. Gamble, H. Taube, T. Satoh and H. Fujii, *Science*, 1998, 280, 560-564.
3. R. Palkovits, M. Antonietti, P. Kuhn, A. Thomas and F. Schüth, *Angew. Chem. - Int. Ed.*, 2009, 48, 6909-6912.
4. B. G. Hashiguchi, C. H. Höverlmann, S. M. Bischof, K. S. Lokare, C. H. Leung and R. A. Periana, in *Energy production and storage: inorganic chemical strategies for a warming world*, ed. R. H. Crabtree, John Wiley, Chichester, 2010, pp. 101 - 141.
5. H. Schwarz, *Angew. Chem. - Int. Ed.*, 2011, 50, 10096-10115.
6. A. Holmen, *Catal. Today*, 2009, 142, 2-8.
7. K. A. Dubkov, V. I. Sobolev and G. I. Panov, *Kinet. Catal.*, 1998, 39, 72-79.
8. E. V. Starokon, M. V. Parfenov, L. V. Pirutko, S. I. Abornev and G. I. Panov, *J. Phys. Chem. C*, 2011, 115, 2155-2161.
9. C. Hammond, M. M. Forde, M. H. Ab Rahim, A. Thetford, Q. He, R. L. Jenkins, N. Dimitratos, J. A. Lopez-Sanchez, N. F. Dummer, D. M. Murphy, A. F. Carley, S. H. Taylor, D. J. Willock, E. E. Stangland, J. Kang, H. Hagen, C. J. Kiely and G. J. Hutchings, *Angew. Chem. Int. Ed.*, 2012, 51, 5129-5133.
10. M. H. Groothaert, J. A. van Bokhoven, A. A. Battiston, B. M. Weckhuysen and R. A. Schoonheydt, *J. Am. Chem. Soc.*, 2003, 125, 7629-7640.
11. N. V. Beznis, B. M. Weckhuysen and J. H. Bitter, *Catal. Lett.*, 2010, 138, 14-22.
12. P. J. Smeets, R. G. Hadt, J. S. Woertink, P. Vanelderen, R. A. Schoonheydt, B. F. Sels and E. I. Solomon, *J. Am. Chem. Soc.*, 2010, 132, 14736-14738.
13. J. Dedecek and B. Wichterlova, *J. Phys. Chem. B*, 1997, 101, 10233-10240.
14. P. E. Fanning and M. A. Vannice, *J. Catal.*, 2002, 207, 166-182.
15. P. Vanelderen, J. Vancauwenbergh, B. F. Sels and R. A. Schoonheydt, *Coord. Chem. Rev.*, 2013, 257, 483-494.
16. S. C. Larsen, A. Aylor, A. T. Bell and J. A. Reimer, *J. Phys. Chem.*, 1994, 98, 11533-11540.
17. J. Sarkany, J. L. Ditri and W. M. H. Sachtler, *Catal. Lett.*, 1992, 16, 241-249.
18. G. T. Palomino, P. Fisicaro, S. Bordiga, A. Zecchina, E. Giamello and C. Lamberti, *J. Phys. Chem. B*, 2000, 104, 4064-4073.
19. V. Umamaheswari, M. Hartmann and A. Pöppl, *The Journal of Physical Chemistry B*, 2005, 109, 1537-1546.
20. M. H. Groothaert, P. J. Smeets, B. F. Sels, P. A. Jacobs and R. A. Schoonheydt, *J. Am. Chem. Soc.*, 2005, 127, 1394-1395.
21. M. LoJacono, G. Fierro, R. Dragone, X. B. Feng, J. dItri and W. K. Hall, *J. Phys. Chem. B*, 1997, 101, 1979-1984.
22. Y. Kuroda, S. Konno, Y. Yoshikawa, H. Maeda, Y. Kubozono, H. Hamano, R. Kumashiro and M. Nagao, *J. Chem. Soc., Faraday Trans.*, 1997, 93, 2125-2130.
23. H. Chen, M. Matsuoka, J. Zhang and M. Anpo, *J. Catal.*, 2004, 228, 75-79.
24. P. J. Smeets, M. H. Groothaert and R. A. Schoonheydt, *Catal. Today*, 2005, 110, 303-309.
25. F. X. Llabrés i Xamena, P. Fisicaro, G. Berlier, A. Zecchina, G. Turnes Palomino, C. Prestipino, S. Bordiga, E. Giamello and C. Lamberti, *J. Phys. Chem. B*, 2003, 107, 7036-7044.
26. H. Yamashita, M. Matsuoka, K. Tsuji, Y. Shioya, M. Anpo and M. Che, *The Journal of Physical Chemistry*, 1996, 100, 397-402.
27. M. Iwamoto, H. Furukawa, Y. Mine, F. Uemura, S. I. Mikuriya and S. Kagawa, *J. Chem. Soc., Chem. Commun.*, 1986, 1272-1273.
28. M. Iwamoto, H. Yahiro, Y. Mine and S. Kagawa, *Chem. Lett.*, 1989, 213-216.
29. C. Lamberti, S. Bordiga, M. Salvalaggio, G. Spoto, A. Zecchina, F. Geobaldo, G. Vlaic and M. Bellatreccia, *J. Phys. Chem. B*, 1997, 101, 344-360.
30. P. Kumashiro, Y. Kuroda and M. Nagao, *J. Phys. Chem. B*, 1999, 103, 89-96.
31. S. Bordiga, E. Groppo, G. Agostini, J. A. van Bokhoven and C. Lamberti, *Chem. Rev.*, 2013, 113, 1736-1850.

32. E. M. Alayon, M. Nachtegaal, M. Ranocchiari and J. A. van Bokhoven, *Chem. Commun.*, 2012, 48, 404-406.
33. E. M. C. Alayon, M. Nachtegaal, A. Bodi and J. A. van Bokhoven, *ACS Catalysis*, 2014, 4, 16-22.
34. J. S. Woertink, P. J. Smeets, M. H. Groothaert, M. A. Vance, B. F. Sels, R. A. Schoonheydt and E. I. Solomon, *Proc. Nat. Acad. Sci. USA*, 2009, 106, 18908-18913.
35. R. L. Lieberman and A. C. Rosenzweig, *Nature*, 2005, 434, 177-182.
36. R. Balasubramanian, S. M. Smith, S. Rawat, L. A. Yatsunyk, T. L. Stemmler and A. C. Rosenzweig, *Nature*, 2010, 465, 115-U131.
37. P. Haack and C. Limberg, *Angew. Chem. Int. Ed.*, 2014, 53, 4282-4293.
38. E. I. Solomon, D. E. Heppner, E. M. Johnston, J. W. Ginsbach, J. Cirera, M. Qayyum, M. T. Kieber-Emmons, C. H. Kjaergaard, R. G. Hadt and L. Tian, *Chem. Rev.*, 2014, 114, 3659-3853.
39. P. P. Y. Chen, R. B. G. Yang, J. C. M. Lee and S. I. Chan, *Proc. Nat. Acad. Sci. USA*, 2007, 104, 14570-14575.
40. S. I. Chan, V. C. C. Wang, J. C. H. Lai, S. S. F. Yu, P. P. Y. Chen, K. H. C. Chen, C.-L. Chen and M. K. Chan, *Angew. Chem. - Int. Ed.*, 2007, 46, 1992-1994.
41. P. P. Y. Chen and S. I. Chan, *J. Inorg. Biochem.*, 2006, 100, 801-809.
42. M. A. Culpepper, G. E. Cutsail, B. M. Hoffman and A. C. Rosenzweig, *J. Am. Chem. Soc.*, 2012, 134, 7640-7643.
43. K. D. Karlin and Y. Gultneh, in *Prog. Inorg. Chem.*, John Wiley & Sons, Inc., 2007, pp. 219-327.
44. W. B. Tolman, *Acc. Chem. Res.*, 1997, 30, 227-237.
45. N. Kitajima, K. Fujisawa, Y. Morooka and K. Toriumi, *J. Am. Chem. Soc.*, 1989, 111, 8975-8976.
46. N. Kitajima, K. Fujisawa, C. Fujimoto, Y. Morooka, S. Hashimoto, T. Kitagawa, K. Toriumi, K. Tatsumi and A. Nakamura, *J. Am. Chem. Soc.*, 1992, 114, 1277-1291.
47. H. Hayashi, S. Fujinami, S. Nagatomo, S. Ogo, M. Suzuki, A. Uehara, Y. Watanabe and T. Kitagawa, *J. Am. Chem. Soc.*, 2000, 122, 2124-2125.
48. S. Mahapatra, V. G. Young, S. Kaderli, A. D. Zuberbühler and W. B. Tolman, *Angewandte Chemie International Edition in English*, 1997, 36, 130-133.
49. M. Mizuno, H. Hayashi, S. Fujinami, H. Furutachi, S. Nagatomo, S. Otake, K. Uozumi, M. Suzuki and T. Kitagawa, *Inorg. Chem.*, 2003, 42, 8534-8544.
50. A. Gunay and K. H. Theopold, *Chem. Rev.*, 2010, 110, 1060-1081.
51. M. F. Qayyum, R. Sarangi, K. Fujisawa, T. D. P. Stack, K. D. Karlin, K. O. Hodgson, B. Hedman and E. I. Solomon, *J. Am. Chem. Soc.*, 2013, 135, 17417-17431.
52. T. N. Sorrell, *Tetrahedron*, 1989, 45, 3-68.
53. K. D. Karlin, Y. Gultneh, J. C. Hayes and J. Zubieta, *Inorg. Chem.*, 1984, 23, 519-521.
54. H. V. Obias, Y. Lin, N. N. Murthy, E. Pidcock, E. I. Solomon, M. Ralle, N. J. Blackburn, Y. M. Neuhold, A. D. Zuberbuhler and K. D. Karlin, *J. Am. Chem. Soc.*, 1998, 120, 12960-12961.
55. N. Kitajima, T. Koda, S. Hashimoto, T. Kitagawa and Y. Morooka, *J. Am. Chem. Soc.*, 1991, 113, 5664-5671.
56. I. Sanyal, M. Mahroof-Tahir, M. S. Nasir, P. Ghosh, B. I. Cohen, Y. Gultneh, R. W. Cruse, A. Farooq and K. D. Karlin, *Inorg. Chem.*, 1992, 31, 4322-4332.
57. P. Haack, A. Kärgel, C. Greco, J. Dokic, B. Braun, F. F. Pfaff, S. Mebs, K. Ray and C. Limberg, *J. Am. Chem. Soc.*, 2013, 135, 16148-16160.
58. P. Vanelderen, R. G. Hadt, P. J. Smeets, E. I. Solomon, R. A. Schoonheydt and B. F. Sels, *J. Catal.*, 2011, 284, 157-164.
59. E. M. C. Alayon, M. Nachtegaal, E. Kleymenov and J. A. van Bokhoven, *Microporous Mesoporous Mater.*, 2013, 166, 131-136.
60. P. Vanelderen, J. Vancauwenbergh, M.-L. Tsai, R. G. Hadt, E. I. Solomon, R. A. Schoonheydt and B. F. Sels, *ChemPhysChem*, 2014, 15, 91-99.
61. R. Frahm, M. Nachtegaal, J. Stotzel, M. Harfouche, J. A. van Bokhoven and J. D. Grunwaldt, *AIP Conference Proceedings*, 2010, 1234, 251-255.
62. D. C. Koningsberger, B. L. Mojet, G. E. van Dorssen and D. E. Ramaker, *Top. Catal.*, 2000, 10, 143-155.
63. M. Vaarkamp, J. C. Linders and D. C. Koningsberger, *Physica B (Amsterdam)*, 1995, 208 & 209, 159-160.
64. A. L. Ankudinov, B. Ravel, J. J. Rehr and S. D. Conradson, *Phys. Rev. B*, 1998, 58, 7565-7576.
65. B. Ravel and M. Newville, *J. Synchroton. Radiat.*, 2005, 12, 537-541.
66. M. J. Frisch, G. W. Trucks, H. B. Schlegel, G. E. Scuseria, M. A. Robb, J. R. Cheeseman, G. Scalmani, V. Barone, B. Mennucci, G. A. Petersson, H. Nakatsuji, M. Caricato, X. Li, H. P. Hratchian, A. F. Izmaylov, J. Bloino, G. Zheng, J. L. Sonnenberg, M. Hada, M. Ehara, K. Toyota, R. Fukuda, J. Hasegawa, M. Ishida, T. Nakajima, Y. Honda, O. Kitao, H. Nakai, T. Vreven, J. J. A. Montgomery, J. E. Peralta, F. Ogliaro, M. Bearpark, J. J. Heyd, E. Brothers, K. N. Kudin, V. N. Staroverov, R. Kobayashi, J. Normand, K. Raghavachari, A. Rendell, J. C. Burant, S. S. Iyengar, J. Tomasi, M. Cossi, N. Rega, J. M. Millam, M. Klene, J. E. Knox, J. B. Cross, V. Bakken, C. Adamo, J. Jaramillo, R. Gomperts, R. E. Stratmann, O. Yazyev, A. J. Austin, R. Cammi, C. Pomelli, J. W. Ochterski, R. L. Martin, K. Morokuma, V. G. Zakrzewski, G. A. Voth, P. Salvador, J. J. Dannenberg, S. Dapprich, A. D. Daniels, Ö. Farkas, J. B. Foresman, J. V. Ortiz, J. Cioslowski and D. J. Fox, in *Gaussian 09, Revision D.01*, Gaussian, Inc., Wallingford CT, 2009.
67. V. Mahadevan, Z. Hou, A. P. Cole, D. E. Root, T. K. Lal, E. I. Solomon and T. D. P. Stack, *J. Am. Chem. Soc.*, 1997, 119, 11996-11997.
68. B. F. Straub, F. Rominger and P. Hofmann, *Chem. Commun.*, 2000, 1611-1612.
69. D. H. Olson, G. T. Kokotailo, S. L. Lawton and W. M. Meier, *J. Phys. Chem.*, 1981, 85, 2238-2243.
70. A. D. Becke, *The Journal of Chemical Physics*, 1993, 98, 5648-5652.
71. S. Grimme, *J. Comput. Chem.*, 2006, 27, 1787-1799.
72. Y. Zhao and D. Truhlar, *Theor. Chem. Acc.*, 2008, 120, 215-241.
73. M. Ernzerhof and J. P. Perdew, *The Journal of Chemical Physics*, 1998, 109, 3313-3320.
74. F. Weigend and R. Ahlrichs, *PCCP*, 2005, 7, 3297-3305.
75. L. E. Roy, P. J. Hay and R. L. Martin, *Journal of Chemical Theory and Computation*, 2008, 4, 1029-1031.
76. J. Tomasi, B. Mennucci and R. Cammi, *Chem. Rev.*, 2005, 105, 2999-3094.
77. L. S. Kau, D. J. Spirasolomon, J. E. Pennerhahn, K. O. Hodgson and E. I. Solomon, *J. Am. Chem. Soc.*, 1987, 109, 6433-6442.

78. C. Lamberti, S. Bordiga, A. Zecchina, M. Salvalaggio, F. Geobaldo and C. O. Arean, *J. Chem. Soc., Faraday Trans.*, 1998, 94, 1519-1525.
79. C. Lamberti, S. Bordiga, F. Bonino, C. Prestipino, G. Berlier, L. Capello, F. D'Acapito, F. Xamena and A. Zecchina, *PCCP*, 2003, 5, 4502-4509.
80. J. M. Tranquada, S. M. Heald and A. R. Moodenbaugh, *Phys. Rev. B*, 1987, 36, 5263-5274.
81. N. Cheng, Y. L. Wei, Y. W. Yang and J. F. Lee, *Phys. Scr.*, 2005, T115, 907-908.
82. J. Chaboy, A. Munoz-Paez, F. Carrera, P. Merkling and E. S. Marcos, *Phys. Rev. B*, 2005, 71.
83. H. R. Oswald, A. Reller, H. W. Schmalle and E. Dubler, *Acta Crystallographica Section C-Crystal Structure Communications*, 1990, 46, 2279-2284.
84. J. B. Forsyth and S. Hull, *J. Phys.: Condens. Matter*, 1991, 3, 5257.
85. G. J. Millar, A. Canning, G. Rose, B. Wood, L. Trewartha and I. D. R. Mackinnon, *J. Catal.*, 1999, 183, 169-181.
86. T. Yumura, M. Takeuchi, H. Kobayashi and Y. Kuroda, *Inorg. Chem.*, 2009, 48, 508-517.

List of Figures *(in a separate document)*

Supporting Information ***(also in a separate document)***

Table 1. Computed 0 K reaction energies in kJ mol^{-1} for the reaction of mono(μ-oxo) complexes to form the bis(μ-oxo) complexes as well as the most stable [**1**-LLM]–O_2 structure as shown in Figure 5(e). In the zeolite model, the disproportionation reaction energies are more relevant and are also given.

Structural type	mono(μ-oxo) to bis(μ-oxo)dicopper reaction	B3LYP					M062X	PBE1hPBE	B97D	M062X
		6-311+G(d)	def2-SVP with LANL2DZ on Cu				def2-TZVP		def2-TZVP with LANL2TZ(f) on Cu	
		(1)	(2)	(3)	(3,4)				(5)	
molecular complex										
	[**2**]–O^{2+} + ½ O_2 → [**2**]–O_2^{2+}	–88	–73	–67	–35		–56	–59	–47	–27
	[**3**]–O + ½ O_2 → [**3**]–O_2	–62	–50	–42	–13	–17	–43	–33	–18	–11
zeolite										
	[**1**-LLM]–O + ½ O_2 → [**1**-LLM]–O_2		10	14			31			
	2 [**1**-LLM]–O → [**1**-LLM]–O_2 + [**1**-LLM]–Ø		275	274			385			

(1) Constrained optimization with Cu-coordinating N atoms frozen at their crystallographic positions. (2) Without ZPE. (3) With ZPE calculated using B3LYP/def2-SVP with LANL2DZ ECP on Cu for [**2**/**3**] and B3LYP/6-311+G(d) for [**1**-LLM]–Ø/O/O_2. (4) In ethanol solution. (5) At the B3LYP/6-311+G(d) optimized geometry

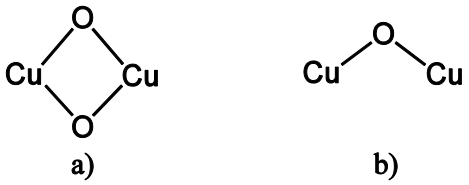

Scheme 1. Illustration of the structures of the a) bis(μ-oxo)dicopper^{III}, and b) mono(μ-oxo)dicopper^{II} cores in copper-zeolites, proposed active for methane activation.

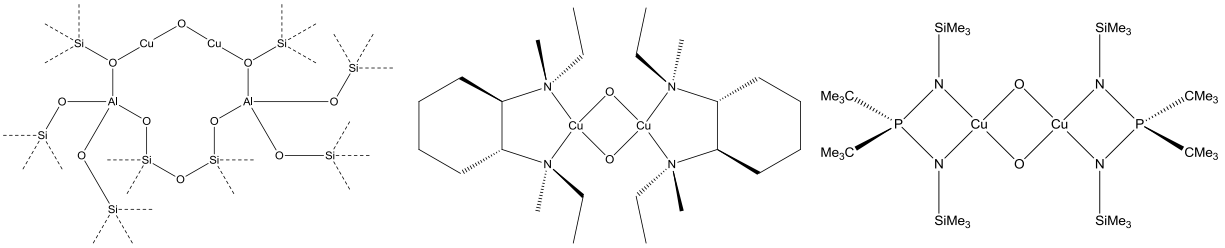

[**1**-LLM]–O [**2**]–O_2 [**3**]–O_2

Scheme 2. Computed structures. In the monooxo large ligand model, the dashed bonds show terminating OH groups. The more stable bis(μ-oxo)dicopper structures are shown for the isolated complexes [**2**/**3**].

a) disproportionation

$$[CuOH]^+ \longrightarrow Cu^+ + OH^\bullet$$
$$[CuOH]^+ + OH^\bullet \longrightarrow H_2O + Cu^{2+}O^-$$
$$2[CuOH]^+ \longrightarrow H_2O + Cu^+ + Cu^{2+}O^-$$

b) condensation

$$2[CuOH]^+ \longrightarrow H_2O + [Cu^{2+}\text{-}O^{2-}\text{-}Cu^{2+}]^{2+}$$
$$[Cu^{2+}\text{-}O^{2-}\text{-}Cu^{2+}]^{2+} \longrightarrow [Cu^+\text{-}[]\text{-}Cu^+] + {}^1/_2O_2$$
$$2[CuOH]^+ \longrightarrow H_2O + [Cu^+\text{-}[]\text{-}Cu^+] + {}^1/_2O_2$$

Scheme 3. Mechanisms proposed in the literature regarding thermal treatment of Cu species in zeolites undergoing autoreduction

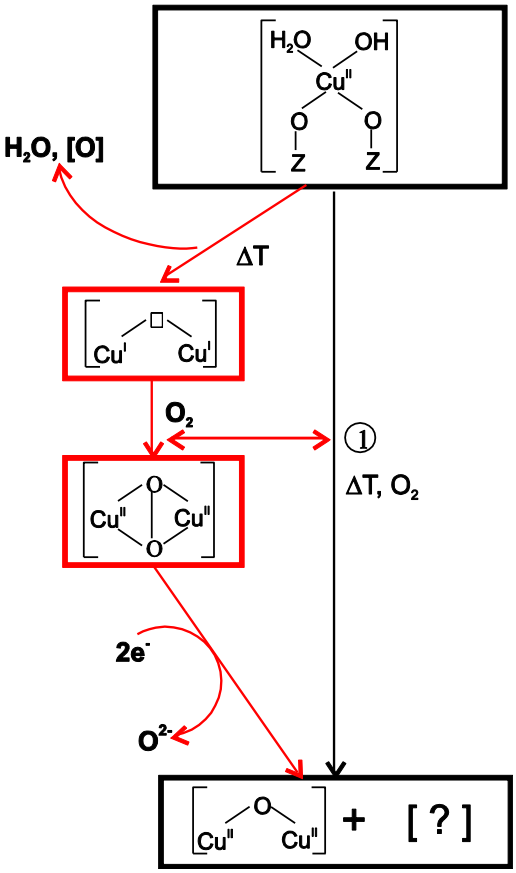

Scheme 4. Chemical scheme of active site synthesis. Thermal treatment of Cu-MOR induces dehydration of the copper sites, which is the driving force for autoreduction. The reduced and undercoordinated copper sites cleave molecular oxygen to form the peroxo precursor, followed by elimination of an oxygen atom to form the active site that activates methane.

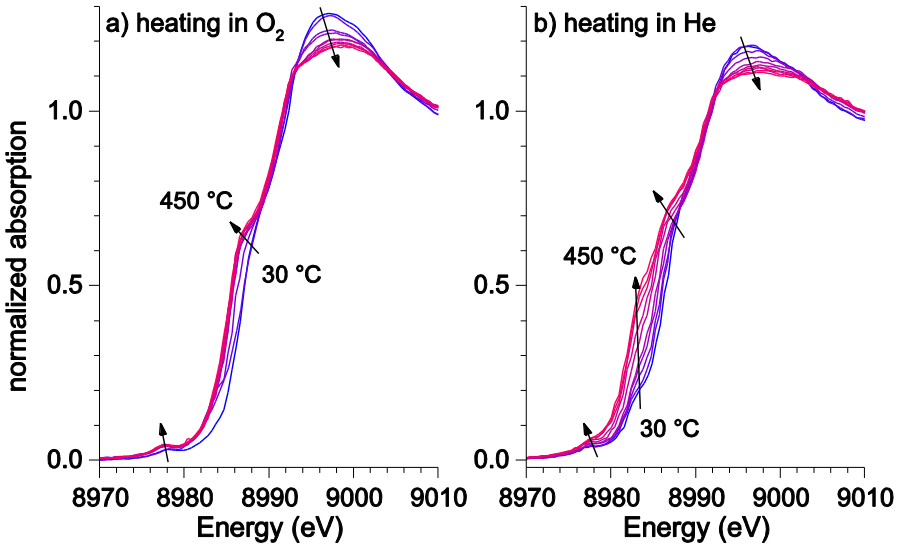

Figure 1. XANES spectra recorded during thermal treatments of Cu-MOR either in a) oxygen or b) helium spaced every 50°C.

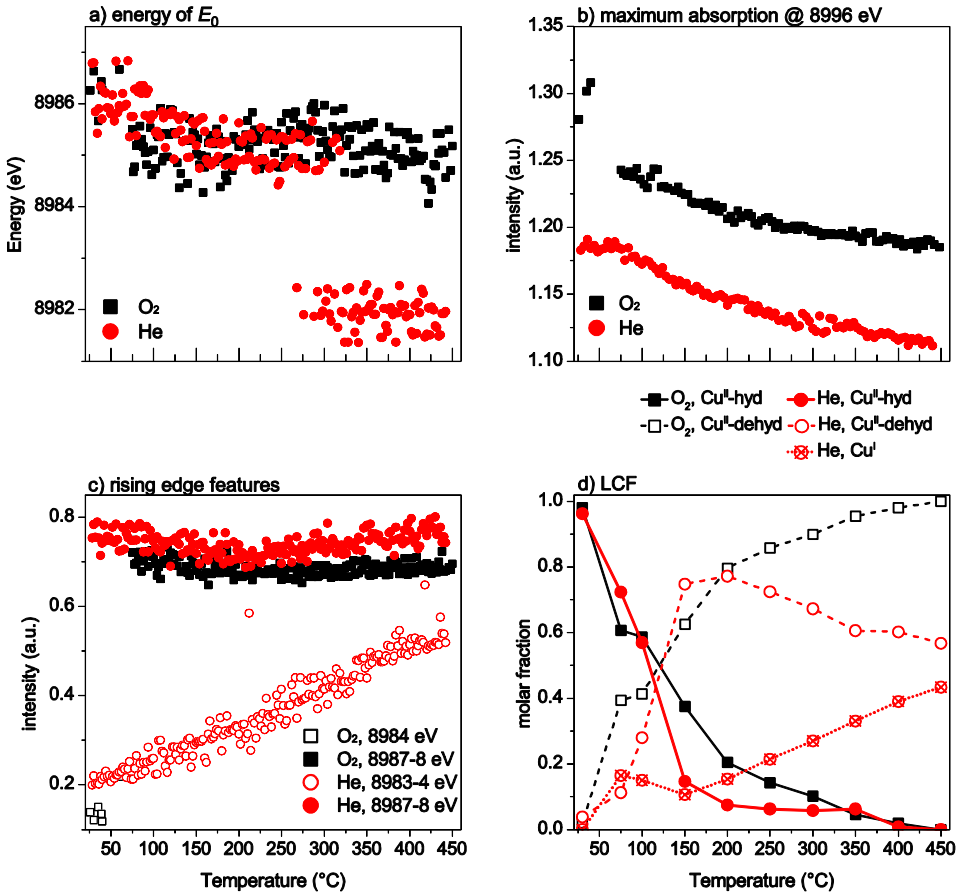

Figure 2. Summary of spectral features during heating either in oxygen or helium a-c), together with d) Linear combination fitting (LCF) results for the XANES (-20 to 50 eV);

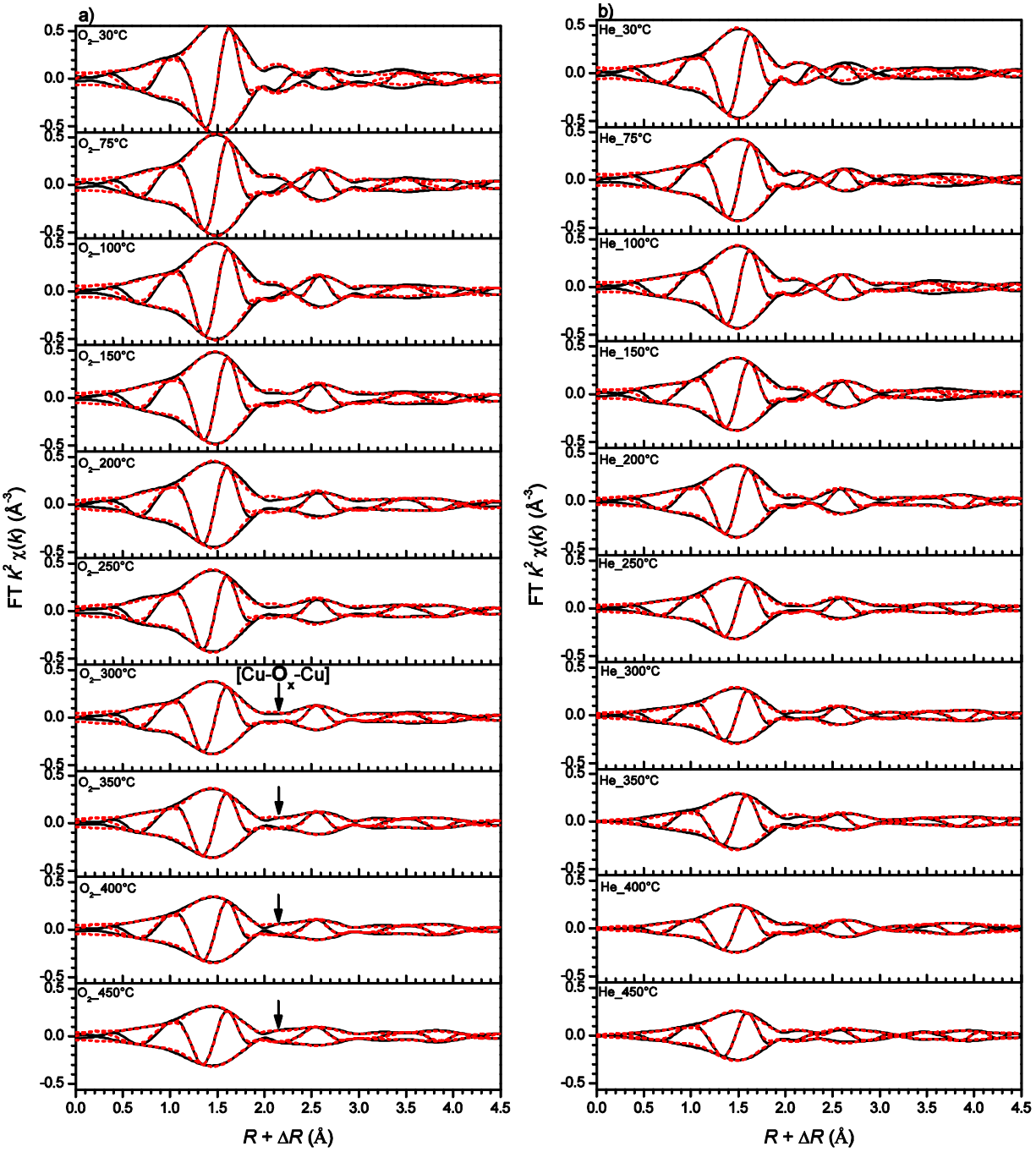

Figure 3. The series of k^2 weighted FT EXAFS spectra and their best fits recorded for Cu-MOR after synthesis and during thermal treatments in (a) oxygen and (b) helium. The arrow (↓) indicates the fitted contribution of oxygen bridging the copper dimer at 2.42 Å, present for the treatment in oxygen and absent for the treatment in helium.

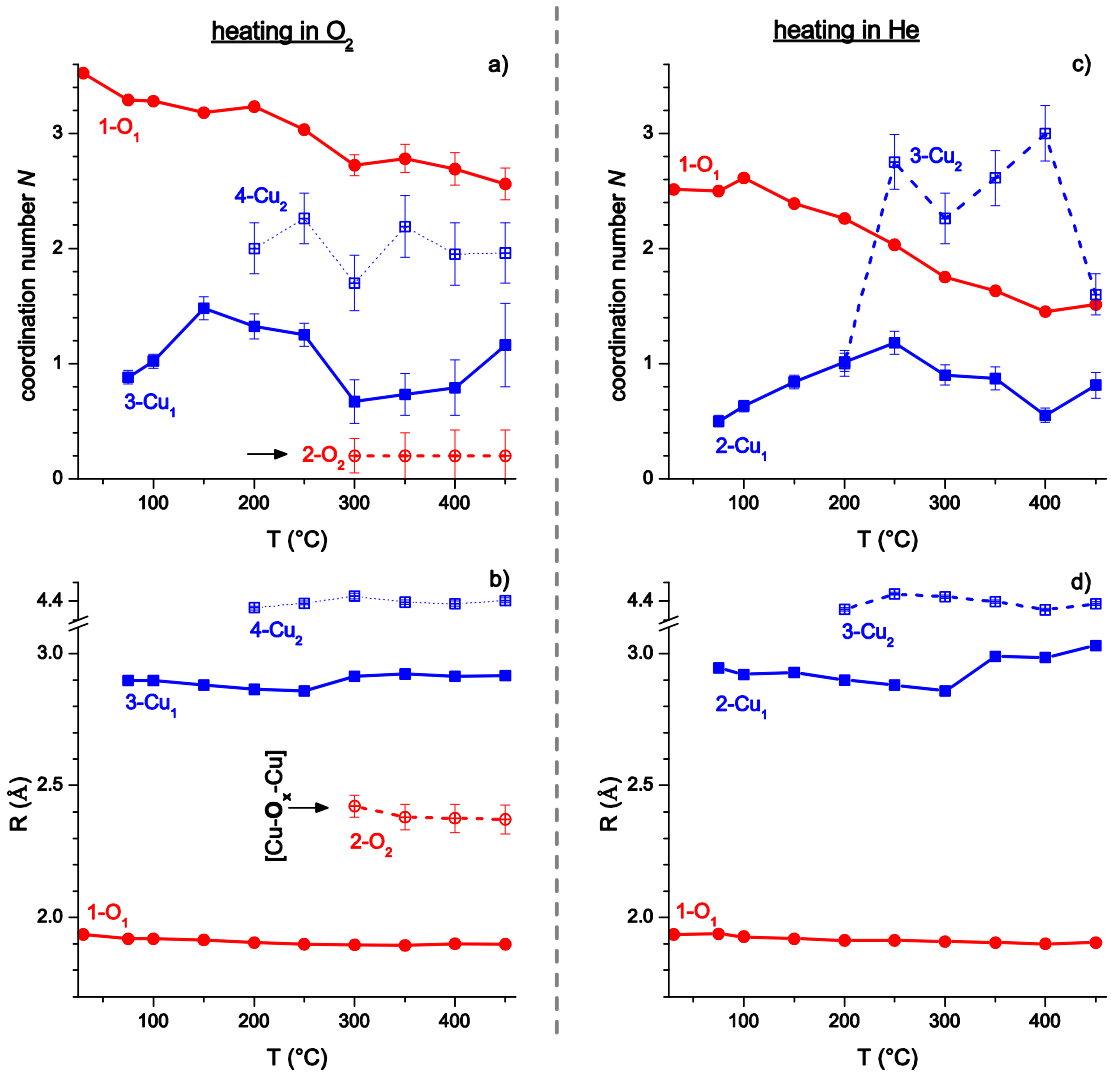

Figure 4. Summary of structural parameters achieved from best fitting of the EXAFS spectra taken of Cu-MOR after synthesis and during thermal treatments in (left) oxygen and (right) helium. The coordination number *N* values in a) correspond to the interatomic distance *R* in b), and so does *N* in c) to the *R* value in d). For the thermal treatment in oxygen, the first, second and third coordination shells were best-fitted to be those of oxygen, oxygen, and copper, respectively, while that in helium were oxygen, copper and copper, in the same order. The arrow (→) indicates the best-fitted contribution of the active oxygen bridging the copper dimer. The numerical results of the fits are displayed in Tables S4-1 and S4-2.

.

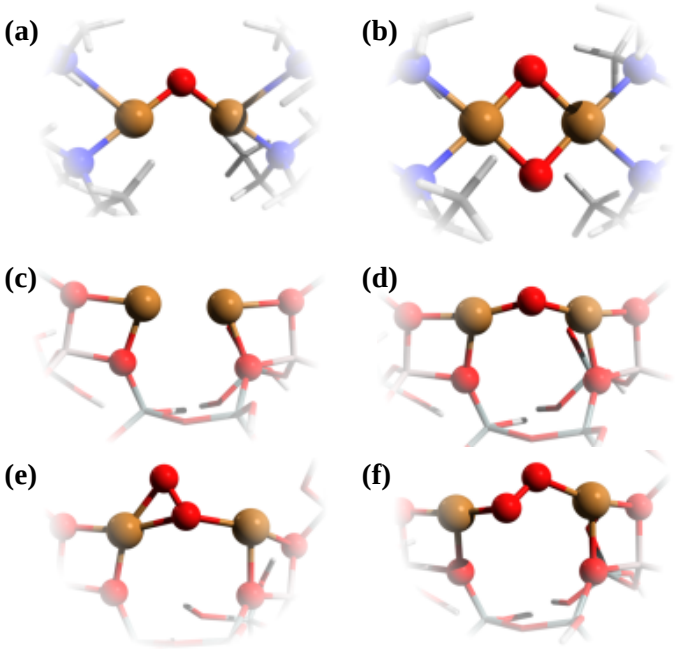

Figure 5. Cu_2O and Cu_2O_2 active sites in (a,b) homogeneous complexes [**2**/**3**] and in (d–f) the zeolite large ligand model [**1**-LLM] as well as (c) the free third-nearest neighbor dicopper site in [**1**-LLM]–Ø. For the full optimized structures see Figure S5-1.